

THE SAMPLE BYU CASIE-09 MICROASAR DATASET

David G. Long and Craig Stringham

Center for Remote Sensing
Brigham Young University
long@ee.byu.edu
Release 1, 1 Oct. 2011

ABSTRACT

This document describes a sample SAR data set collected by the BYU/Artemis microASAR system as flown as part of the Characterization of Arctic Sea Ice Experiment 2009 (CASIE-09). This data set is made available as a public service to the wider community to further interest in low-cost SAR applications. Sample Matlab scripts to process the data set into images using both the range-Doppler algorithm and the backprojection algorithm are also provided. This document, the sample data, processed images, and Matlab scripts that illustrate the processing are provided at URL http://www.mers.byu.edu/microASAR/CASIE_sample/. The appropriate citation for the data set is “microASAR [1] data courtesy of David G. Long at Brigham Young University [2].” To help justify further funding from our sponsors, a copy of any publication using this data or software is requested. Please send to long@ee.byu.edu.

1. INTRODUCTION

In the summer of 2009, a small, low power SAR was flown on a small, unmanned aircraft system (UAS) as part of the Characterization of Arctic Sea Ice Experiment 2009 (CASIE-09) [3] over the Arctic Ocean from Svalbard Island. The goal of the mission was to measure ice roughness in support of research into monitoring ice thickness and ice age. The C-band SAR instrument, known as microASAR, collected 19.8 hours of high resolution SAR image data over 32.4 hours of UAS flight time in six UAS flights of varying length. The UAS was the NASA Sensor Integrated Environmental Remote Research Aircraft (SIERRA) [4]. As configured for operation on CASIE-09, the microASAR [1] collected data to on-board flash disk for later processing on the ground. The full dataset is considered proprietary. However, in the interest of furthering the application of SAR systems, a sample raw SAR data set from this mission is being made available for research. This document briefly describes the microASAR, the data set, and provides some examples of the processed processed images. The reader is assumed be familiar with SAR processing, see [5] for a good tutorial on SAR

processing algorithms. For specific information on LFM-CW SAR processing see [6] and [7].

2. MICROASAR AND THE SIERRA UAS

Synthetic aperture radar (SAR) can be a useful tool for sea ice observation, but SAR sensors have traditionally been large and expensive. The compact microASAR builds on the design of the BYU microSAR [8], but is a much more robust and flexible system [1]. The microASAR uses a linear frequency-modulated continuous-wave (LFM-CW) transmit signal generated by a direct digital synthesizer (DDS) chip. The system is pseudo-monostatic, i.e., it transmits and receives at the same time using two separate antennas that are placed closely together. This enables long transmit chips which maximize the SNR while minimizing peak transmit power. The return signal is mixed down with a frequency-shifted copy of the transmit signal (this is known as analog dechirp), digitized, and processed with an all-digital final IF stage. Internal filtering minimizes transmit/receive signal feedthrough. Raw data is stored to compact flash (CF) disk along with GPS timing and position data. Using 32 GB CF disks, over two hours of SAR data can be recorded. Table 1 provides a summary of the microASAR hardware specifications. For the CASIE experiment, the microASAR transmit bandwidth is set to 170 MHz, yielding a maximum ideal range resolution of approximately 90 cm, though the effective resolution is reduced in processing. The transmit center frequency is 5.42876 GHz. After hardware presumming, the effective PRF is 307.292 Hz.

A key goal of CASIE-09 is to provide fine spatial resolution over difficult to access locations in the high Arctic. Satellites cannot provide the desired simultaneous combination of sensor types and resolution. Piloted aircraft typically fly too high and too fast to yield the fine-scale sampling rates and mapping patterns required by our project. UAS-based measurements can be made at low speed and low altitude in dangerous Arctic conditions without putting humans in manned aircraft at risk.

In CASIE-09 a microASAR was flown aboard the NASA SIERRA UAS. With a relatively large payload capacity, efficient mission planning software, and in-flight programmable autopilot, the SIERRA is well-suited for the long-duration missions used in the CASIE-09 experiment. Some of the other sensors on the UAS included two optical cameras, two pyrometers, an up/down-looking shortwave spectrometer, high-quality inertial measurement unit (IMU), and a laser profilometer system consisting of two down-pointing lasers, a medium-quality IMU, and differential-capable GPS receiver [1].

The UAS provided GPS position data via a serial data stream to the microSAR where it was included in the data storage. During CASIE-09 a video camera was mounted to view in the same direction as the microASAR, providing optical imagery coincident with the SAR swath (this data is not included with the sample data set). The UAS was flown at low altitude, typically between 600' and 1500'. While the low altitude limits the microSAR swath width, it also benefits the SAR measurement SNR. The low altitude operation results in an extremely wide range of incidence angles across the obseration swath.

The processed CAISE-09 SAR images show a variety of surface features from open

Physical Specifications	
Supply Power	< 35 W
Supply Voltage	+15 to +26 VDC
Dimensions	22.1×18.5×4.6 cm
Weight	2.5 kg
Radar Parameters	
Transmit Power	30 dBm
Modulation Type	LFM-CW
Operating Frequency Band	C-band
Transmit Center Frequency	5428.76 MHz
Signal Bandwidth	80-200 MHz (variable)
PRF	7-14 kHz (variable with optional hardware presumming)
Radar Operating Specifications	
Theoretical Resolution	0.75 m (@ 200 MHz BW)
Operating Velocity	10-150 m/s
Operating Altitude	500-3000 ft
Swath Width	300-2500 m (alt. dependent)
Collection Time (for 10GB)	30-60 min (PRF dependent)
Antennas (2 used)	
Type	2 × 8 Patch Array
Gain	15.5 dB (peak)
3dB Beamwidth	11° (Azimuth) × 42° (Elevation)
Size	35 × 12 × 0.25 cm

Table 1. General microASAR Specifications

ocean to dense pack ice. Features visible in the SAR imagery, as confirmed by the corresponding video, include ridges, rubble fields, brash ice, leads, and melt ponds. A particular microASAR image is shown in Fig. 1.

3. MICROASAR DATA

The microASAR can be programmed for operation in different modes and resolutions. For CASIE-09 raw data is divided into 1 min segments and separately processed into multi-looked image segments typically 3.5 km long in the along-track dimension by 1.2 km wide in the cross-track dimension. The sample data set provided here consists of a 13 sec portion of one of these segments (segment 9, collected on 25 July 2009), which was arbitrarily selected. Figure 2 shows a screen shot of a GoogleEarth window illustrating the full image segment shown as a georectified image. The sample data set corresponds to a portion near the center of the image. Due to the low altitude operation, the far-range is at an extreme incidence angle, and is thus not useful due to low SNR. (This area appears bright due to range compensation in this image.) The primary observation swath is defined to be from

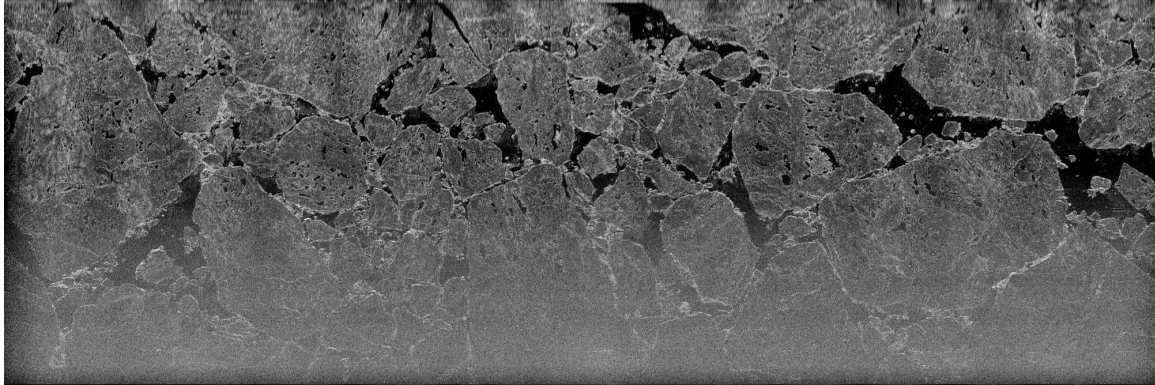


Fig. 1. Sample microASAR image from CASIE-09. Nadir is along the top. The UAS flew from left to right, viewing the surface to the right of the flight track as viewed from the aircraft (downward in the figure). The incidence angle varies from zero at the top to well over 72° at the bottom of the image. The image has been range compensated. Most of the surface is covered with ice floes with the dark areas corresponding to open water and melt ponds. The vertical banding is caused by antenna gain variations due to periodic rolling motion of the UAS. The image shows an area approximately 3.5 km long by about 1.2 km wide.

just off nadir to an incidence angle of about 72 deg. Many of the images shown later are clipped to this incidence angle range. Note that the surface is essentially flat and at sea-level for this data set. The average horizontal velocity during the sample data set collection is 30.1938 m/s at an average height of 346.5029 m.

For distribution the sample CASIE-09 microASAR data is provided in a single Matlab “MAT-file”, “flight9_9_sample.mat”, containing arrays for the sampled raw dechirped data (named “dat”) and the geometry data (named “geom”). Each of the 3885 columns of the arrays “dat” and “geom” represent the dechirped SAR data and the aircraft location interpolated for each pulse, respectively. The four rows of “geom” are the SAR pulse number, latitude in degrees, longitude in degrees, and altitude in m.

The following describes microASAR details and settings as used for the CASIE-09 experiment for the sample data set and how the data can be processed into images. Additional detail can be found in the sample Matlab processing scripts.

After digital IF processing in the microASAR hardware, the effective sample rate of the dechirped data is 24.485 MHz. To maximize the SNR for CASIE, the microASAR was set to use a high rate repeating chirp (i.e., a high PRF) with a LFM frequency ramp rate of $1.5972563681 \times 10^{12}$ Hz/s. To reduce the data rate for the CASIE-09 experiment onboard storage, the microASAR employed hardware presumming, which consists of coherently averaging several sequential pulses together, resulting in an effective PRF of 307.292 Hz (see [9] for additional detail).

Recall that in an LFM-CW radar range compression can be accomplished by computing a zero-padded FFT of each LFM chirp. (Technically, the microASAR is not strictly CW, as there are small gaps between the individual transmitted chirps, though this does not

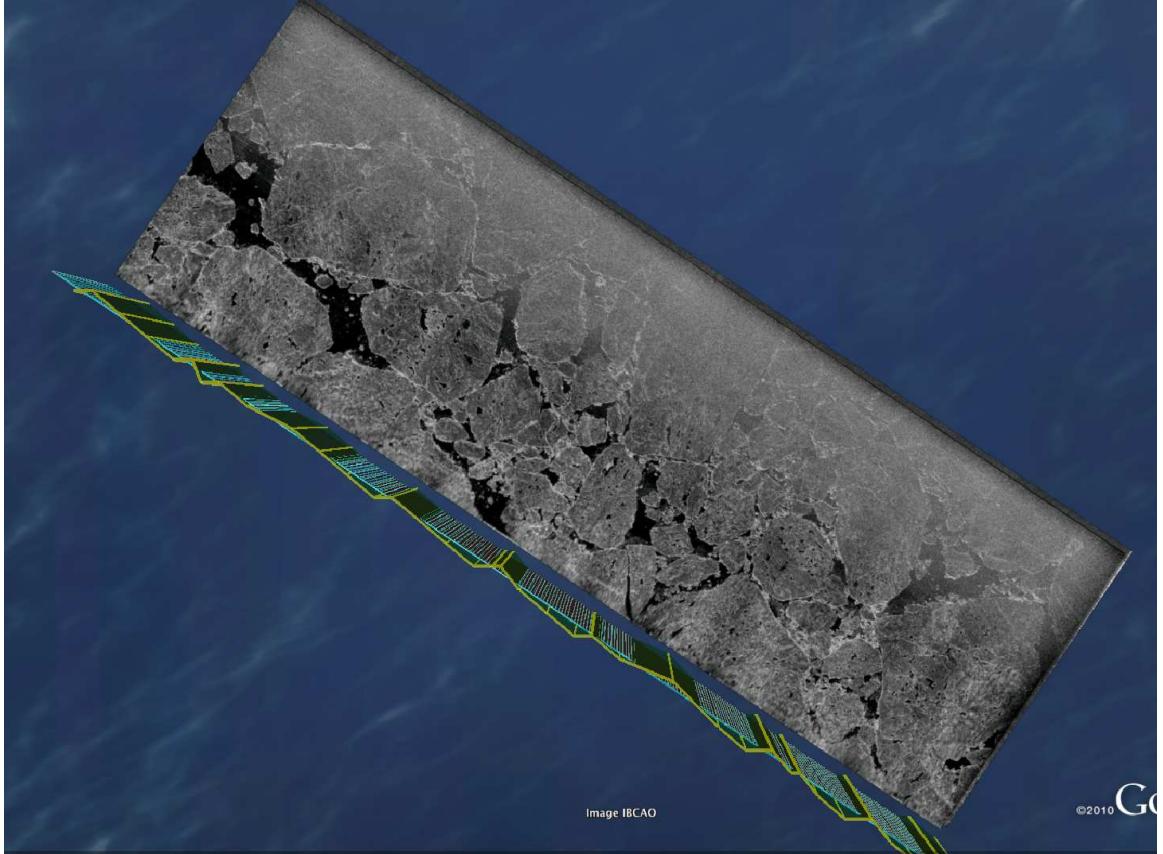


Fig. 2. Image segment 20090725_9 shown as a backprojected image in GoogleEarth. The UAS flight track is indicated with the blue path and nadir is along the bottom. MicroASAR-recorded GPS positions are in yellow. The UAS flew from lower-right to upper-left, viewing the surface to the right. The incidence angle varies from zero at nadir track near GPS track to over 72° at the top of the SAR image.

alter the processing.) In range compressing the CASIE microASAR data note that the start portion (the first 30 samples) of each LFM chirp (for convenience a single LFM chirp is referred to as a ‘pulse’) should be zeroed to avoid artifacts induced by transient RF signals caused by the switching of the transmitter. The dechirped pulse length is truncated to 1702 dechirped samples prior to onboard storage. Note that zeroing and truncation have the side effect of reducing the theoretical range resolution of the range compressed data to 1.35 m/sample. After zero-padding each chirp to 4096 values and computing the FFT, the redundant negative frequency half of the range compressed data can be discarded.

Figure 3 shows the range-compressed image created from the sample dataset. Note that zero padding changes the meters per pixel in the range-compressed image, though the effective resolution is unchanged. In this image the nadir return occurs at approximately range bin 800 in this example. Range bins prior to the nadir return (which are in the blue area at the top of the image) contain no useful information. The primary swath shows as red and light blue. The internal cabling delay corresponds to approximately 1.2 m. For this

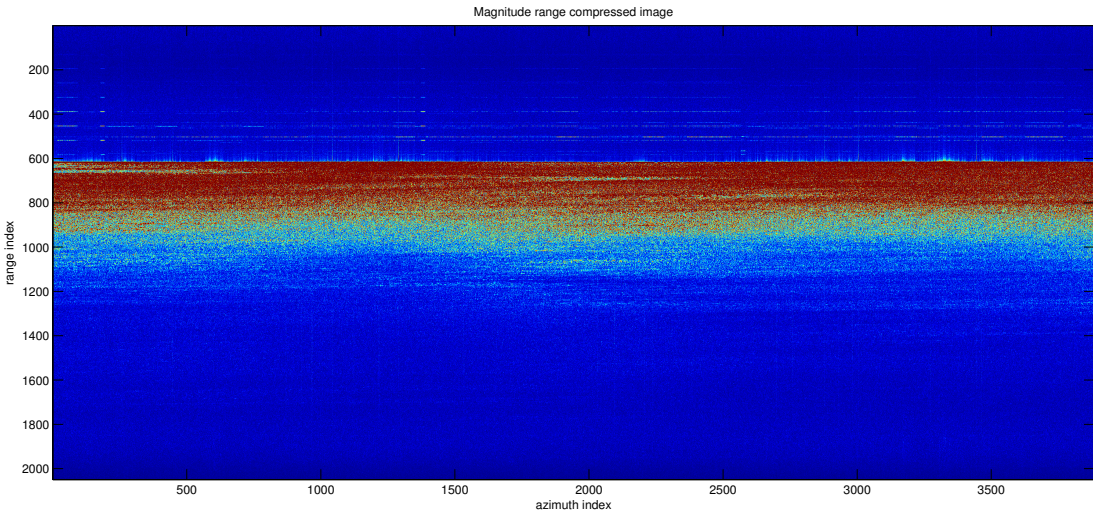


Fig. 3. Magnitude images of the range-compressed sample data set computed by zero padding and using a 4096 point FFT. Nadir is at the top of the red area and the platform moves from left to right.

data collection, the platform height offset described in [2] has already been applied to the GPS altitude data recorded in the geom array.

Each pulse has a unique pulse counter number. Due to limitations of the data storage system there are occasional missing pulses. These can be identified by gaps in the sequential pulse counter. For range-Doppler processing such gaps need to be filled (e.g., by interpolation) to avoid introducing azimuth artifacts. See Matlab code for details.

4. SAR IMAGE FORMATION

To encourage further research and development of SAR imaging techniques, we include a Matlab script, “casie_sample.m” that creates focused SAR images of the sample data set using the range Doppler algorithm (RDA) and backprojection. Note that azimuth compression of an LFM-CW SAR includes an additional phase term compared to a conventional pulsed SAR system, see [6] and [7].

4.1. Range Doppler Processing

In the range-Doppler algorithm, a range-dependent azimuth filter is required to minimize aliasing and the effects of the platform’s rapid attitude variation. An example of a single-look azimuth compressed image created using RDA without range migration or motion compensation is shown in Fig. 4. To approximately compensate for range roll-off in this image, the image pixel values are scaled by r^3 . In addition the images are displayed in Decibels with an arbitrarily selected grayscale range. No compensation for the antenna

gain pattern is included. Note that the backscatter response from sea ice is incidence angle dependent, but this is not compensated for. In this and following images, the image is clipped to nadir at the left and an incidence angle of 72° at the right.

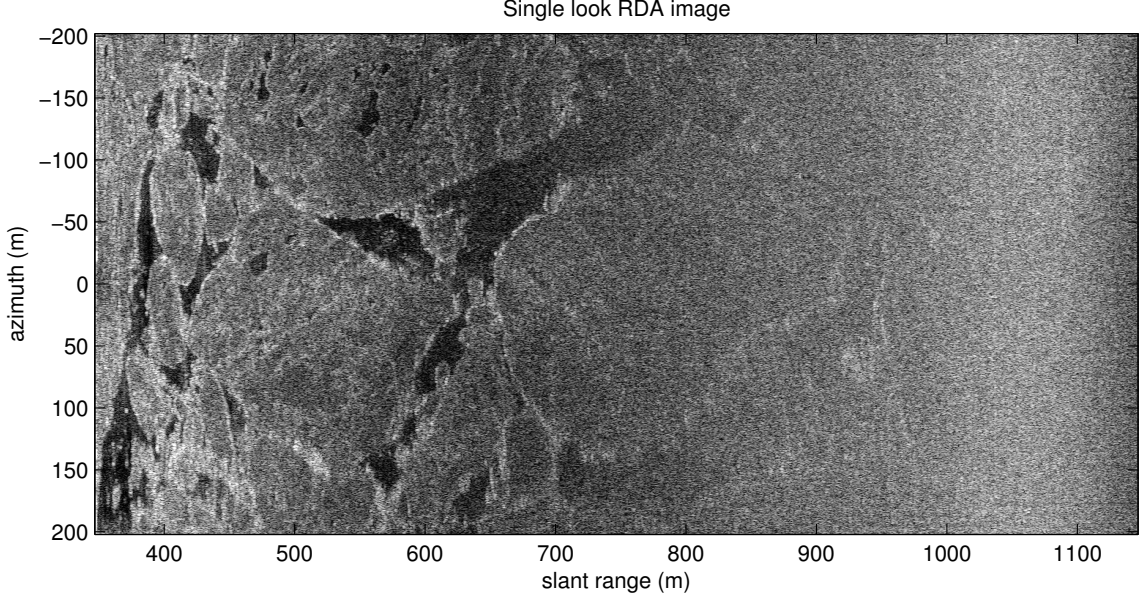


Fig. 4. Magnitude of the single look azimuth-compressed complex image. (Note that the image is compressed vertically to display it here. This has the effect of making the displayed image appear multi-looked and reducing the appearance of speckle.)

To optimize the focus when creating the RDA image using the low altitude CASIE data we find it advantageous to use a hyperbolic azimuth chirp rather than the traditional RDA parabolic azimuth chirp. A conventional parabolic azimuth chirp $Az(m)$ used for RDA azimuth compression at range r_a can be expressed as

$$Az(m) = \exp \left\{ -j \left(\frac{f_c m^2 v^2}{c r_a \text{PRF}^2} - \frac{2 f_c v^2 m}{c^2 \text{PRF}} \right) \right\} \quad (1)$$

where $m = [-N_p/2..N_p/2]$ is the pulse index where N_p is the number of pulses, f_c is the carrier frequency, c is the speed of light, PRF is the pulse repetition frequency, and v is the along-track velocity. For a hyperbolic version, we define

$$\tau(m) = 2\sqrt{r_a^2 + (mv/\text{PRF})^2} \quad (2)$$

where the azimuth displacement is mv/PRF and

$$Az(m) = \exp \left\{ -j \left(2\pi f_c \tau(m) + K_r \tau^2(m) \right) \right\} \quad (3)$$

where K_r is the LFM frequency ramp rate. Of course, an appropriate azimuth window should be applied.

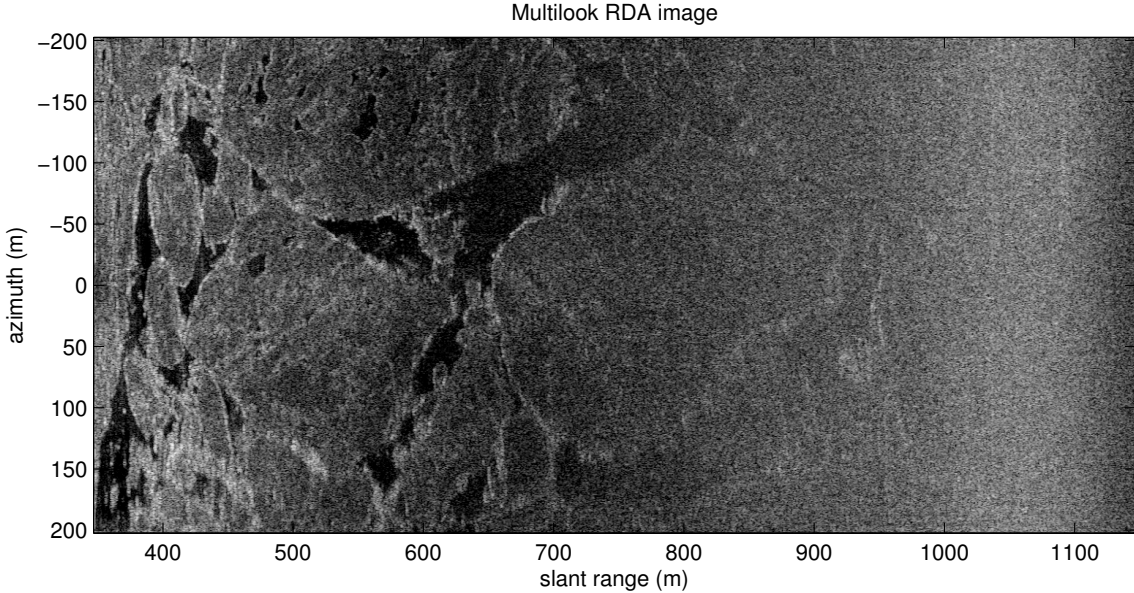


Fig. 5. Magnitude of the multi-looked RDA image.

Since the single look azimuth resolution ($1/2$ the antenna length) is much smaller than the range resolution, spatially square pixels can be generated by generating an image with high azimuth resolution and incoherently averaging (multi-looking) pixels in the azimuth direction to reduce the azimuth resolution and speckle noise. A multi-looked (in azimuth) image generated from the image in Fig. 4 shown in Fig. 5. There is a reduction in the speckle level and the increased contrast in the multi-looked image.

Note that Figs 4 and 5 are in slant range. Using the multi-looked azimuth compressed image and the height information an example of a georectified image is shown in Fig. 6. This is in cross-track distance, or ground range, i.e. it represents a map view from above. For this image a simple nearest-neighbor range interpolation is used to convert from slant range to ground range. The low altitude emphasizes the variations in range resolution of the ground range image. Note the expected effective resolution loss in range resolution near nadir.

4.2. Backprojection Processing

Backprojection is a deceptively simple approach for generating images from raw synthetic aperture radar (SAR) data. SAR backprojection implements the azimuth matched filter for each pixel, and accounts for both range cell migration and the motion of the aircraft.

The time domain backprojection algorithm is an exact algorithm for creating images from SAR data. The algorithm computes the radar cross-section over a grid of pixels in ground range on the surface. For a pixel located (x_0, y_0, z_0) , the SAR backprojection algorithm for an LFM-CW radar can be approximately expressed as [7]

$$A(x_0, y_0) = \sum_n S(n, d[n]) P(d[n]) \exp\{-j4\pi(d[n]/\lambda - d^2[n]K_r/c^2)\} \quad (4)$$

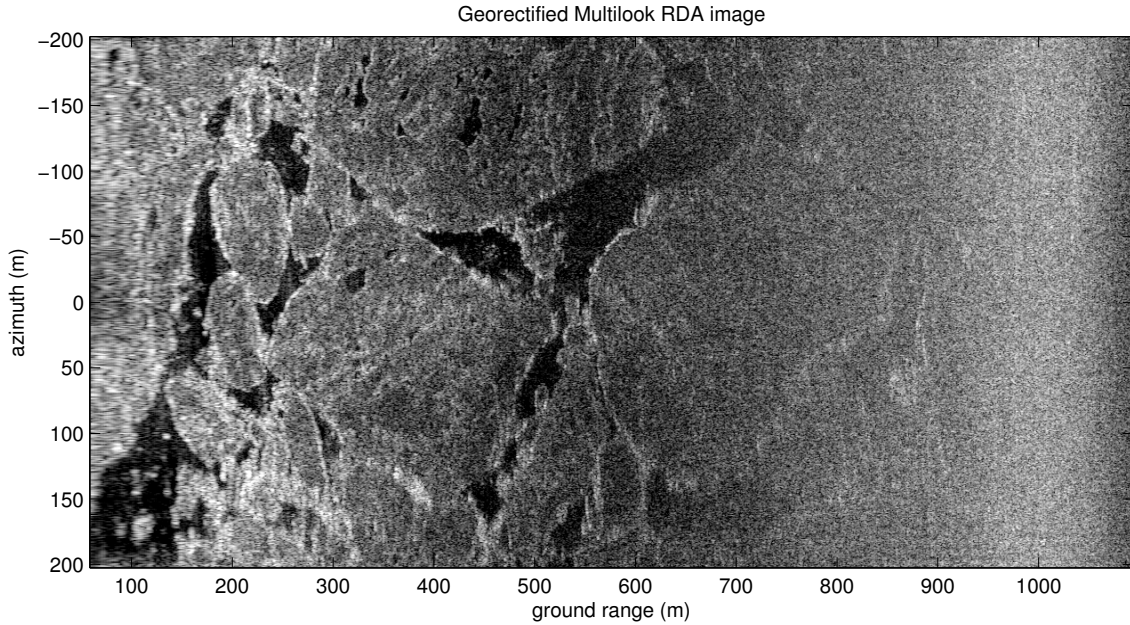


Fig. 6. Georectified RDA magnitude image. (normally the left few image lines would be clipped from the image).

where $A(x_0, y_0)$ is the complex pixel value (the complex SAR image), λ is the wavelength of the transmit frequency at the center of the SAR band, $d[n]$ is the distance between (x_0, y_0, z_0) and the antenna phase center of the SAR antenna $(x[n], y[n], z[n])$ for pulse number n . The distance $d[n]$ is defined as

$$d[n] = \sqrt{(x[n] - x_0)^2 + (y[n] - y_0)^2 + (z[n] - z_0)^2}. \quad (5)$$

A range-dependent azimuth window $S(n, d[n])$, which is pulse index (n) dependent, is included in the processing to enable subaperture processing and/or reduce azimuth sidelobes. In Eq. (4) $P(d[n])$ is the range-compressed SAR data interpolated to slant range $d[n]$. The summation is over the pulses which for which the azimuth and elevation gain of the antenna are significant. An image is created by varying the horizontal positions x_0 and y_0 over a grid. The height z_0 of the surface at (x_0, y_0) is typically computed from a digital elevation map (DEM). Since the CASIE-09 images are at the surface $z_0 = 0$.

The challenge of time-domain backprojection is that it is computationally intensive; however it can be parallelized to achieve near real-time performance in many cases as described in [2]. While the implementation of backprojection included in the Matlab code sample uses Matlab GPU constructs in order to speed up the processing if a GPU is available, the implementation of the backprojection algorithm provided in the sample code is written for simplicity and clarity rather than computational efficiency. The implementation includes the phase term required to compensate for motion of the platform during the transmit pulse for an LFM-CW SAR as described in [7].

Single and multi-look images generated using backprojection are shown in Fig. 7 and Fig. 8. Note that the backprojected images are inherently in ground range, i.e. they are georectified. We note an increase in visible detail in comparison to the images generated with RDA due to the fact that backprojection accounts for range migration and platform motion.

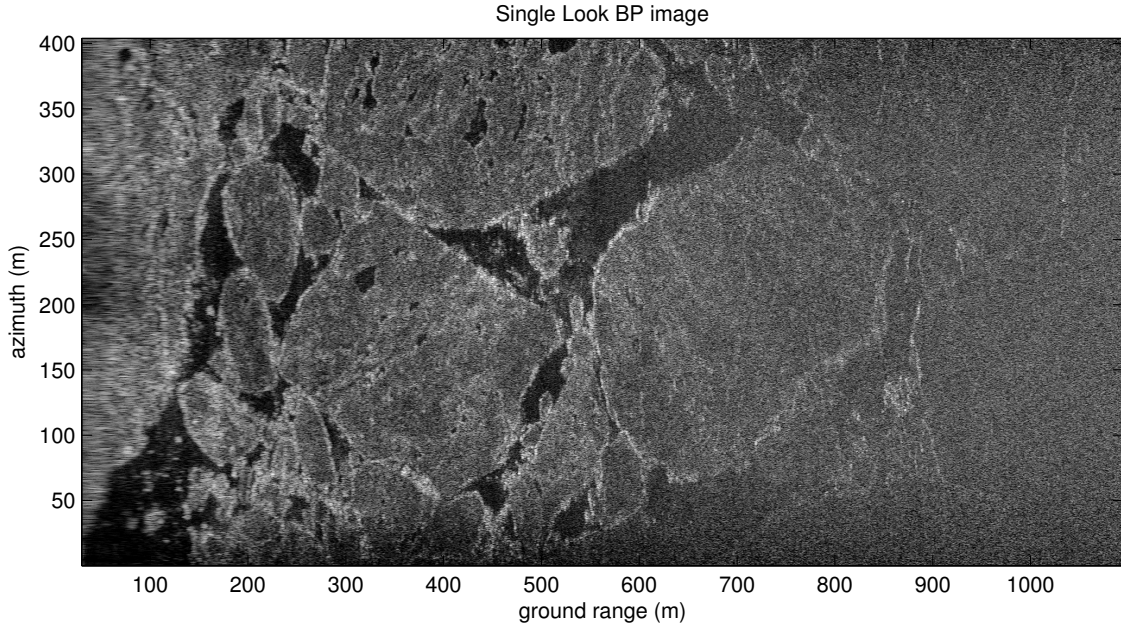


Fig. 7. Magnitude of the single look backprojection complex image. (Note that the image is compressed vertically to display it here. This has the effect of making the displayed image appear multi-looked and reducing the appearance of speckle.)

5. REFERENCES

- [1] M. Edwards, D. Madsen, C. Stringham, A. Margulis, B. Wicks, and D. Long, “microASAR: A small, robust LFM-CW SAR for operation on UAVs and small aircraft,” *IEEE International Geoscience and Remote Sensing Symposium, 2008*, vol. 5, July 2008.
- [2] C. Stringham and D. G. Long, “Improved processing of the CASIE SAR data,” *IEEE International Geoscience and Remote Sensing Symposium (IGARSS), 2011*, July 2011.
- [3] J. Maslanik, R. Crocker, K. Wegrzyn, C. Fowler, U. Herzfeld, D. Long, R. Kwok, M. Fladeland, and P. Bui, “Characterization of Fram Strait sea ice conditions using the NASA SIERRA unmanned aircraft system,” *AGU Fall Meeting Abstracts*, vol. 1, 2009, p. 06.

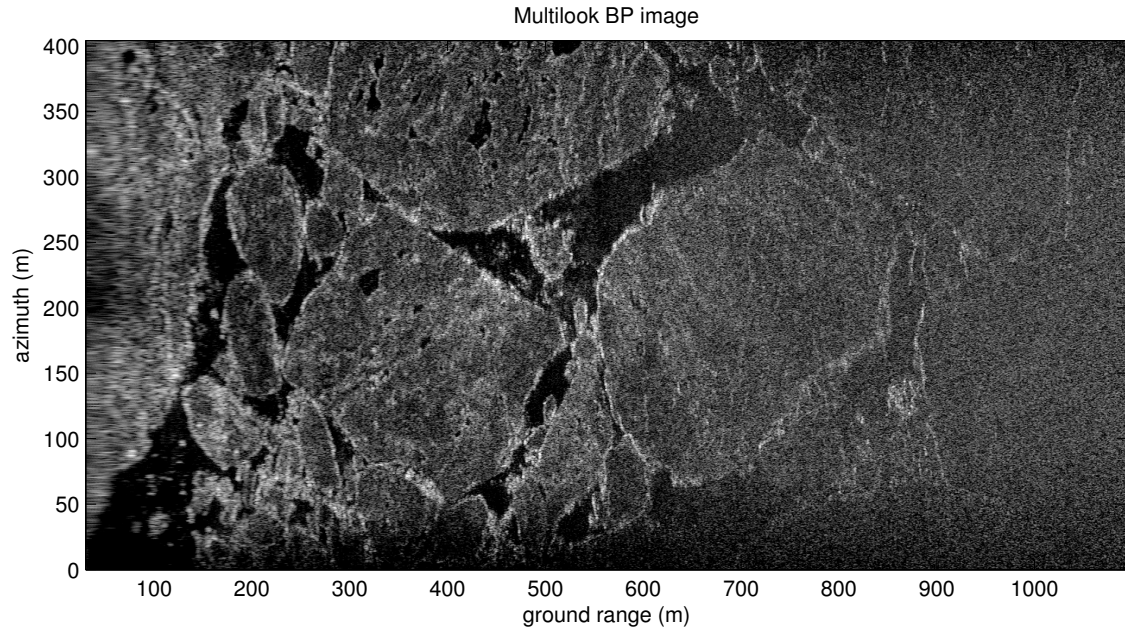


Fig. 8. Magnitude of the multi-looked backprojection image.

- [4] M. Fladeland, R. Berthold, L. Monforton, R. Kolyer, B. Lobitz, and M. Sumich, “The NASA SIERRA UAV: A new unmanned aircraft for earth science investigations,” *AGU Fall Meeting Abstracts*, vol. 1, 2008, p. 0365.
- [5] I. G. Cumming and F. H. Wong, *Digital Processing of Synthetic Aperture Radar Data*, Norwood, MA: Artech House, 2005.
- [6] E. Zaugg and D. Long, “Theory and application of motion compensation for LFM-CW SAR,” *IEEE Transactions on Geoscience and Remote Sensing*, vol. 46, no. 10, pp. 2990–2998, 2008.
- [7] E. Zaugg and D. G. Long, “Generalized LFM-CW SAR processing,” *IEEE Transactions on Geoscience and Remote Sensing*, in review, 2010.
- [8] E. Zaugg, D. Hudson, and D. Long, “The BYU SAR: A small, student-built SAR for UAV operation,” *IEEE International Conference on Geoscience and Remote Sensing Symposium*, Aug. 2006, pp. 411–414.
- [9] C. Stringham and D. G. Long, “Digital receiver design for an offset IF LFM-CW SAR,” *Proceedings of Radar Conference (RADARCON) 2011*, pp. 960-964, 23-27 May 2011.